

Apertureless Tip-Enhanced Raman Microscopy with Confocal Epi-Illumination/Collection Optics

DMITRY S. BULGAREVICH and MASAYUKI FUTAMATA*

Nanoarchitectonics Research Center, National Institute of Advanced Industrial Science and Technology, Tsukuba Central 4, 1-1-1 Higashi, Tsukuba 305-8562, Japan

It is demonstrated that confocal epi-illumination/collection optics can be effectively used to generate surface-enhanced Raman scattering at the near-field region of a gold-coated tip for an atomic force microscope operated in semi-contact tapping mode. When the tip, with a 50-nm apex radius, was illuminated by a highly focused laser beam at 532 nm and approached the isolated diamond particle, with a size of $\sim 1 \mu\text{m}$, the Raman signal was enhanced by $\sim 10^3$. This result is in good agreement with numerical simulations performed by the finite difference time-domain method. Since our apertureless microscope is based on readily available conventional components, there is wide room for improvements and modifications by common users in various applications of micro-Raman analysis.

Index Headings: **Tip-enhanced Raman spectroscopy; Scanning near-field Raman spectroscopy; Surface-enhanced Raman scattering; Finite difference time-domain method.**

INTRODUCTION

One of the recent microscopy techniques to overcome the Abbe limit on optical resolution is so-called "apertureless" scanning near-field optical microscopy (SNOM). Potentially, it could provide chemical fingerprinting with nanometer-size spatial resolution and single molecule sensitivity, which obviously has far-reaching implications. In the case of Raman spectroscopy, the basic idea of such apertureless scattering-type near-field microscopy is to use laser illumination to generate a highly concentrated electric field (E) at the tip. If the dimensions of such a tip are on the nanometer scale, then the tip can act as an effective nanometer-size light source at its near-field region. When a sample is placed in this region, the well-known phenomena of surface-enhanced Raman scattering (SERS) could be produced.¹⁻³ Then, it is possible to collect SERS signals by ordinary far-field optics. Depending on the tip-to-sample separation distance, the wavelength of the laser light and its incident angle, tip apex geometry, and the material of the tip and sample, surface plasmon resonance,⁴ lightning rod,⁵ image field,⁶ and chemical^{7,8} enhancement effects are involved in the enhancement. Since SERS signal intensity is approxi-

mately proportional to the E^4 , in principle it is possible to obtain Raman spectra with single molecule sensitivity and spatial resolution determined by the tip apex size.^{9,10} In addition, if a cantilever for an atomic force microscope (AFM) is used as an apertureless probe, both the surface topography and the corresponding chemical composition of the sample can be obtained simultaneously. Prior to the apertureless technique, another near-field Raman microscopy technique was developed during the last decade. It is based on optical fiber probes with subwavelength apertures manufactured by chemical etching and metal overcoating,¹¹⁻¹⁵ which provides promising spatial resolutions of approximately 20–30 nm.¹⁶ However, apertureless probes have, in principle, much higher spatial resolution^{10,17} and excellent scattering (collection) efficiency over the optical fiber.^{18,19} Electromagnetic field enhancement at the tip apex depends on many factors such as tip material and its geometry, as well as the illumination configuration.^{10,20,21} Also, unwanted background scattering from the tip shaft and sample, as well as cantilever heating by laser light, could pose an experimental problem.

In recent years, several optical configurations of such apertureless Raman microscopes have been tested and described in the literature. For example, a total internal reflection (TIR) illumination/collection scheme through the same oil immersion objective was developed.²²⁻²⁴ Similarly, but without TIR, epi-illumination/collection optics, which produced a highly focused laser beam at the tip position, was also used.^{25,26} In addition, side illumination/collection schemes^{27,28} and side illumination, epi-collection configurations^{29,30} were tested. Our confocal epi-illumination/collection scheme belongs to this family of apertureless Raman microscopes. Besides obvious limitations attributed to this technique such as sample transparency, it has several advantageous points useful for particular applications. First of all, confocal configuration will produce a tight focal point and very small light collection volume, which should suppress unwanted background far-field scattering from the sample and tip shaft. At the same time, the position of the focal plane is adjustable to achieve maximum Raman signal enhancements. Also, the epi-illumination/collection scheme does not generate shadowing from the tip. In addition, the ap-

Received 14 November 2003; accepted 27 February 2004.

* Author to whom correspondence should be sent. E-mail: m.futamata@aist.go.jp.

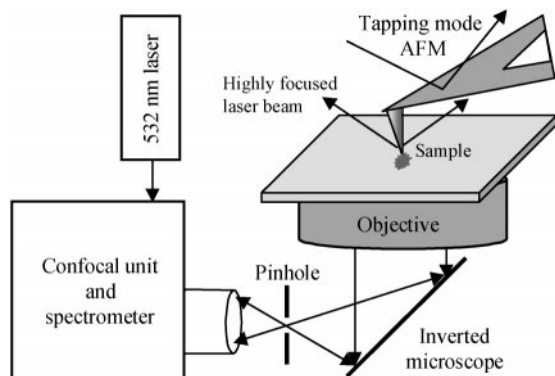


Fig. 1. Confocal experimental setup for generation and observation of tip-enhanced Raman scattering (see text for details).

paratus could be based on ready available commercial components, which require minimum user adaptation.

In this short paper, we report the basic design of our apertureless tip-enhanced Raman microscope. The apparatus is tested by observing the enhanced Raman signal from synthetic monocrystalline diamond powder using the gold-coated AFM cantilever. In addition, it is shown that experimental enhancement factors agree well with our numerical simulations based on the finite difference time-domain (FDTD) method.³¹

EXPERIMENTAL

Figure 1 shows the basic experimental setup. A gold-coated cantilever (NSG 20/Au, NT-MDT) installed on a stand-alone AFM (SMENA, NT-MDT) was illuminated by a 532 nm laser (Coherent, DPSS 532) beam. The cantilevers used here have the following geometrical parameters: apex radius of 50 nm, cone angle of $<22^\circ$, ~ 50 nm thickness of coated Au film, and tip height (distance between the tip apex and shaft) of 10–20 μm . The preference for gold over silver coating was due to the higher chemical stability of gold, although both metals possibly have the resonance wavelength for the localized surface plasmon close to our excitation wavelength (532 nm), e.g., 520 nm for an isolated gold sphere with a radius of 40 nm, or approximately 510 nm for a silver ellipsoid of 140 nm \times 140 nm \times 60 nm. The illumination was done through the objective (UMPlanFl, NA = 0.95, 100 \times , WD = 0.31 mm) of an Olympus IX-70 inverted microscope by using a confocal unit (Nanofinder, Tokyo Instruments, Inc). The scattered light was collected with the same objective and pinhole ($\phi = 60 \mu\text{m}$) and directed to the polychromator and charge-coupled device (CCD) (ANDOR) for spectral analysis. As a sample material, we used synthetic monocrystalline diamond powder (Sigma-Aldrich, approximate size of 1 μm , purity of 99.9%) on the microscope cover-slip surface.

In a typical experiment, the AFM cantilever was roughly located above the single diamond particle. For this aim, the CCD camera attached to the microscope eyepiece and connected to a computer was used. Then, repeated AFM scans in semi-contact mode were conducted to confirm the steadiness of the particle, its sufficient separation from others ($>5 \mu\text{m}$), and its topography. After that, the cantilever tip was positioned above the area of interest by means of the AFM software. Next,

by moving the microscope stage, on which the AFM head and sample were placed, the confocal laser spot and cantilever tip were superimposed. Intensified light scattering from the tip and particle manifested good coincidence. To achieve this, another CCD camera with a tele-objective focused on the cantilever from the side proved to be indispensable for speedy alignment. Also, the coincidence between the cantilever tip and the laser spot, as well as the good focusing conditions, were confirmed by the intensified brightness of the sample field of view through the pinhole. Finally, background corrected Raman spectra were measured with 90 s accumulation time for 2 mW laser power at the sample position. The cantilever drift above the sample for our open-loop AFM scanner was about 200 nm per 10 min.

Three-dimensional FDTD simulation³¹ was used to evaluate the local electric field intensity formed near the gold cantilever. In this calculation, we adopted a tip apex radius of 40 nm, a cone angle of 20° , and excitation by a plane wave at 540 nm with an incident angle of 45° , having *p*- or *s*-polarization (see Fig. 4). Mesh sizes of 2 nm gave sufficient accuracy for the field intensity. The incident angle was close to the average angle produced by our “dry” objective, so the geometrical model corresponded to our experimental conditions and could be compared with reported data.¹⁰ The dielectric constant of gold at 540 nm ($\epsilon = -6.29 + 2.04i$) was taken from the literature.³² Other computational procedures were similar to our previously reported simulations of local fields on silver nanoparticles.³³

RESULTS AND DISCUSSION

Figure 2A shows a topographic image of the investigated diamond particle by using the gold-coated cantilever. The black mark represents the laser spot and the initial tip position above the particle for Raman measurements. In Fig. 2B, the corresponding Raman spectra for the approached (in semi-contact mode) and vertically withdrawn (by $\sim 50 \mu\text{m}$) cantilever are presented. Figure 2C depicts Raman spectra from the diamond particle at different relative positions (*x*, *y*) of the tip. Clearly, there was significant increase in Raman band intensity from the diamond at $\sim 1330 \text{ cm}^{-1}$ when the tip was located within the tight confocal laser spot. Similar results were also observed with other gold-coated cantilevers and diamond particles (not shown). The increased background level seen in our figures for the cantilevers approaching the sample is due to the tail of the broad emission spectrum from the AFM laser (see Fig. 1, $\lambda = 670 \text{ nm}$, $I = 0.9 \text{ mW}$). Also, somewhat different Raman signal intensity for the tip returned back to the (0, 0) position (see Fig. 2C) is due to the accuracy of our AFM open-loop scanner.

These results can be compared to experiments with a bare Si cantilever (NSC11, NT-MDT) used as the probe. For this tip, the radius of curvature is less than 10 nm, its height is 15–20 μm , and the cone angle is less than 20° . As seen from Fig. 3A, the investigated particle was almost twice as thick compared to the particle depicted in Fig. 2A, and thus it produced a stronger Raman signal even for the withdrawn position. However, repeated approach of the tip did not generate significant enhancement

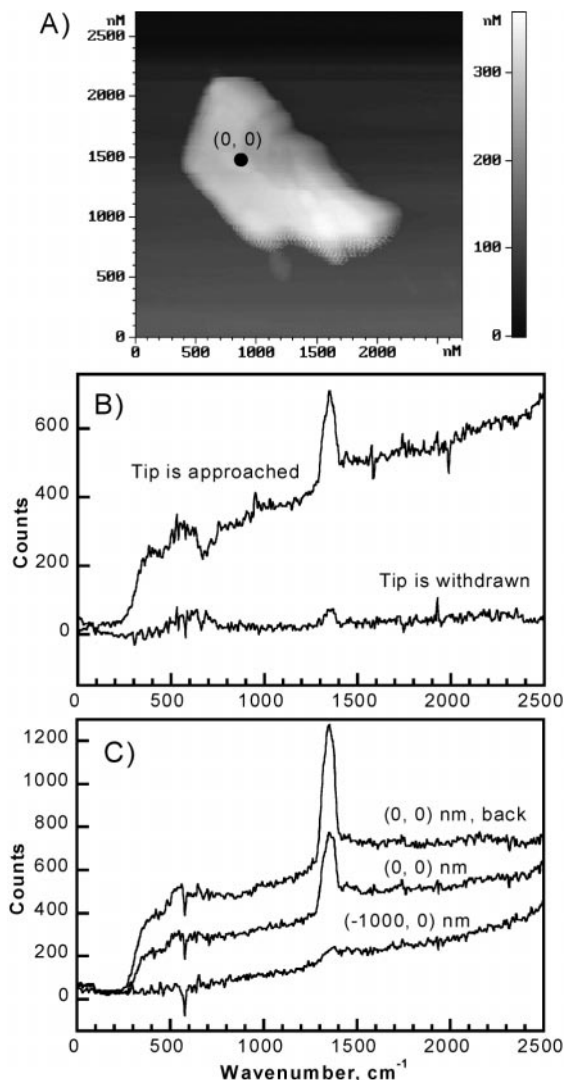


FIG. 2. (A) Surface topography and Raman spectra of diamond micro-particle as a function of different (B) vertical and (C) horizontal positions of the gold-coated AFM cantilever. The black spot corresponds to the initial cantilever tip position in semi-contact mode, and numbers in brackets represent the tip (x, y) coordinates.

of the Raman signal for different diamond particles (as an example, see Fig. 3B). It only led to the disappearance of the Raman signal from the Si tip at $\sim 520 \text{ cm}^{-1}$. This can be seen more clearly in Fig. 3C. By moving the Si tip away from the laser spot and diamond particle, the Si signal progressively decreased in contrast to the intact Raman signal from the diamond. These results allow us to confirm that the SERS effect of the gold-coated cantilever is responsible for the observed enhancement in the near-field Raman signal from the diamond sample.

Using the results for the intensity ratio, $I_{\text{near field}}/I_{\text{far field}} \approx 5$, from Fig. 2B and the simple cylindrical model for the confocal light collection volume for the sample and the near-field volume under the tip to provide effective light scattering, the enhancement factor, EF , for the Raman signal was evaluated as follows:

$$EF = \frac{I_{\text{near field}}}{I_{\text{far field}}} \frac{V_{\text{far field}}}{V_{\text{near field}}} \approx 5 \times \frac{120^2 \times 520 \text{ nm}^3}{50^2 \times 20 \text{ nm}^3} \approx 750$$

Since Raman signal intensity was roughly proportional

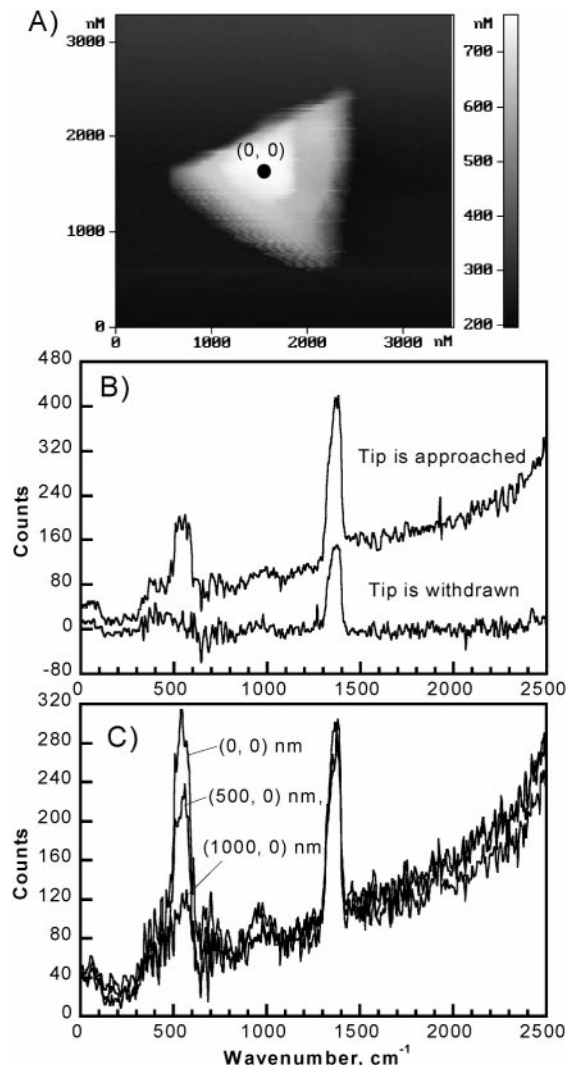


FIG. 3. (A) Surface topography and Raman spectra of diamond micro-particle as a function of different (B) vertical and (C) horizontal positions of Si AFM cantilever. The black spot corresponds to the initial cantilever tip position in semi-contact mode, and numbers in brackets represent the tip (x, y) coordinates.

to E^4 , the electric field enhancement (EFE) under our gold-coated tip was ~ 5 . In the above equation, it was supposed that the base radius of the cylinder for confocal light collection corresponded to the confocal lateral resolution, $r_{\text{far field}} \approx 1.22\lambda/(4\sqrt{2}NA) \approx 120$, where $\lambda = 532$ and $NA = 0.95$ were our laser light wavelength and numerical aperture of the objective, respectively. Next, it was also assumed that Raman signal from the diamond came only from the half height of the cylinder for confocal light collection volume, which corresponded to the confocal axial resolution, $h_{\text{far field}} = 1.77\lambda/[2(NA)^2] \approx 520 \text{ nm}$.³⁴ Regarding the light scattering cylinder at the near-field region under the tip, we set its base radius to the tip apex radius, $r_{\text{tip}} = 50$, and its height, $h_{\text{near field}}$, to 20 nm.

To validate our experimental observations, we also used numerical solving of Maxwell's equations by the FDTD method. The illuminated gold-coated tip was modeled in three-dimensional geometrical conditions relevant to the conducted experiments. Figure 4 shows the cross-section of the electric field obtained for the laser illumination, k , propagated from the bottom with an incident

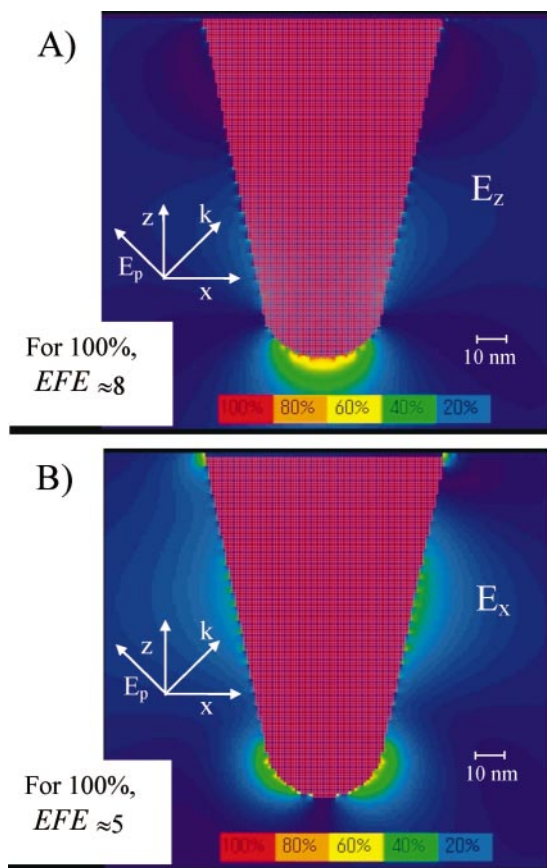


FIG. 4. Cross-section of electric field enhancement and its distribution around the gold-coated AFM tip illuminated by p -polarized light (E_p): (A) E_z component and (B) E_x component with respect to the incident field. See text for more details.

angle of 45° with respect to the z axis. The incoming electric vector E with p - or s -polarization is orthogonal to k . Figures 4A and 4B represent the enhanced electric field for the z and x components with p -polarization. As seen from Fig. 4A for the E_z component, EFE was about 8 at the tip surface and 4 at a distance of 10 nm from the tip apex. In the case of E_x (see Fig. 4B), there were no enhancements directly under the tip, though the EFE was about 3 at 10 nm distance from the tip at opposite edges along the x axis. For s -polarization (not shown), both the E_z and E_y components did not generate EFE directly under the tip apex. However, modest EFE of ~ 3 was observed at the opposite edges of the tip surface. Since in our experiments we did not control precisely the polarization of the light, and the tip was not strictly perpendicular to the sample surface, all three components (E_z , E_x , and E_y) of p - and s -polarization could contribute to the Raman signal enhancements. Note also the good similarity between our experimental (~ 5) and computational values of EFE .

Our results can also be compared with previously reported experimental values of EF ,^{24–26,28–30} which were about 10^3 – 10^4 , when other apertureless Raman microscopes were used. Thus, typical EFE under different AFM cantilever tips were between ~ 5 and 14. It is also interesting that various optical configurations produced very similar results. The possible explanation could be drawn from recent finite-element frequency-domain

(FEFD) method simulation of the field distribution for AFM tip-enhanced Raman microscopy ($\lambda_{\text{laser}} = 810$ nm, silver or golden tips).¹⁰ Note that in all tested experimental configurations, high numerical aperture objectives or geometry of illumination can produce sufficiently high incident angles (45° – 90°) of the laser beam relative to the tip long axis, though, according to simulations, this translates to only $\sim 30\%$ variation in EFE . The tip apex diameters between 10 and 100 nm, laser excitation wavelengths between 485 and 810 nm, and Ag or Au coating of the tips also produced only minor deviations experimentally and computationally. However, for tip-to-sample separation distances between 200 and 0 nm, EFE could increase by one order of magnitude.

Such moderate enhancements observed by using different apertureless Raman microscopes can be compared with the enormous factors, up to 10^{15} , known for molecules adsorbed on metal nanoparticles.⁹ As a result, more efficient involvement of lightning rod, surface plasmon resonance, and other SERS effects is needed by adjusting the morphology of metal-coated probes. In addition, future experimental improvements of apertureless Raman microscopes are in the efficiency of light collection, quality of AFM tips, resolution, and scanning functions.

Here it is worth mentioning several complications that we encountered in our experiments. On one occasion, a small diamond particle was accidentally attached to the cantilever tip during AFM scanning (not laser trapped). In this case, positioning of the tip in the laser focus above the clean cover-slip still produced diamond Raman signal. This particle was probably very small, because there was no measurable effect of such contamination on cantilever resonance frequency. However, Raman signal intensity from such a nanoparticle was comparable to that for larger microparticles (compare Figs. 5A and 2B). Since the particle was in direct contact with the tip surface, and because the main enhancements are from the fixed near-field region of the tip apex, this explains the observed similarity. On the other hand, picking up minute amounts of sample on the cantilever tip (for example, from evaporated liquid solution), basically could be a useful technique for Raman microanalysis.

Another complication was aging of the cantilever tip apex. After several tens of AFM scans, the gold-coated cantilever tips stopped producing measurable enhancements. Figure 5B shows typical results obtained with an aged tip, which originally generated strong enhancements (see Fig. 2). Also, only a fraction of the commercial gold-coated cantilevers were suitable for the apertureless Raman microscopy. Some of them had insufficient gold coating on the Si surface, as is easily seen by comparing the relative intensity of the Si band for active (see Fig. 2) and inactive (see Fig. 5C) tips. It was also reported in the literature that usually only a fraction (5–40%) of the silver or gold-coated cantilever tips had good qualities.^{26,27}

CONCLUSION

It was shown that confocal epi-illumination/collection optics could be used to generate comparatively strong Raman signal enhancements under the tip apex of a gold-coated AFM cantilever. In principle, this could lead to

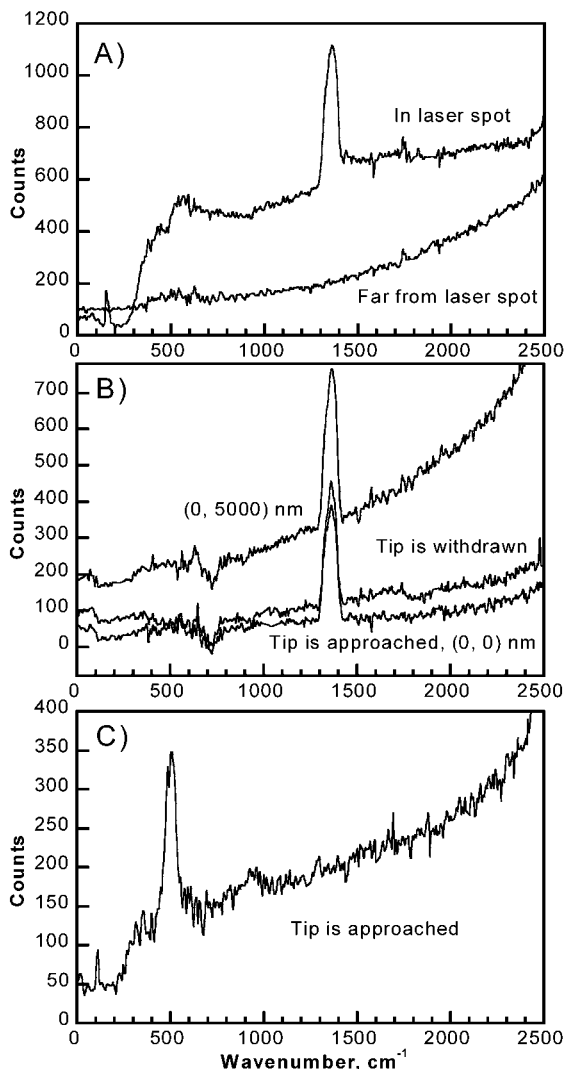


FIG. 5. Different experimental complications: (A) attachment of diamond nanoparticle to the AFM tip, (B) tip aging, and (C) insufficient tip quality (see text for details).

the construction of a Raman microscope that combines all the advantages of scanning confocal and apertureless near-field microscopy. The confocal scheme effectively rejected much of the far-field light compared to simple epi-illumination/collection optics. As a result, we were able to observe significant differences in the Raman signal intensity from diamond samples (even with $\sim 1 \mu\text{m}$ thickness) between approached and withdrawn tip positions. Note that previous reports with the epi-illumination/collection scheme were limited to very thin samples with less than $\sim 10 \text{ nm}$ thickness.^{25,26} Thus, our apparatus opens the possibility for wider practical applications. Compared to reported TIR configurations,^{22–24} much thicker samples can be studied with our microscope. Here it should be stressed that we used the semi-contact mode in contrast to the contact mode reported in TIR experiments. In addition, there was no need to use any additional metal film under the sample, which complicates sample preparation and data interpretation. Also, our scheme allows focal plane adjustment to illuminate effectively the particular cantilever tip. Next, compared to

the side-illumination scheme,^{27–30} we didn't observe dramatic increase in enhancement factors, and reasons for that were discussed above. However, our confocal epi-illumination/collection scheme can accommodate conventional AFM scanners on top of confocal inverted microscopes. It is more user friendly, e.g., it has larger flexibility to add additional optical and mechanical components. Still, as does any confocal system, our apparatus has obvious limitations in sample transparency.

1. A. Campion and P. Kambhampati, *Chem. Soc. Rev.* **27**, 241 (1998), and references therein.
2. M. Moskovits, *Rev. Mod. Phys.* **57**, 783 (1985), and references therein.
3. A. Otto, I. Mrozek, H. Grabhorn, and W. Akemann, *J. Phys.: Condens. Matter* **4**, 1143 (1992), and references therein.
4. J. I. Gersten and A. Nitzan, *J. Chem. Phys.* **73**, 3023 (1980), and references therein.
5. J. I. Gersten, *J. Chem. Phys.* **72**, 5779 (1980).
6. G. C. Schatz and R. P. Van Duyne, *Surf. Sci.* **101**, 425 (1980).
7. J. R. Lombardi, R. L. Birke, T. Lu, and J. Xu, *J. Chem. Phys.* **84**, 4174 (1986).
8. P. Kambhampati, C. M. Child, M. C. Foster, and A. Campion, *J. Chem. Phys.* **108**, 5013 (1998).
9. S. Nie and S. R. Emory, *Science* (Washington, D.C.) **275**, 1102 (1997).
10. M. Micic, N. Klymyshyn, Y. D. Suh, and H. P. Lu, *J. Phys. Chem. B* **107**, 1574 (2003).
11. D. P. Tsai, A. Othonos, M. Moskovits, and D. Uttamchandani, *Appl. Phys. Lett.* **64**, 1768 (1994).
12. C. L. Jahncke, M. A. Paesler, and H. D. Hallen, *Appl. Phys. Lett.* **67**, 2483 (1995).
13. D. A. Smith, S. Webster, M. Ayad, S. D. Evans, D. Fogherty, and D. Batchelder, *Ultramicroscopy* **61**, 247 (1995).
14. C. L. Jahncke, H. D. Hallen, and M. A. Paesler, *J. Raman Spectrosc.* **27**, 579 (1996).
15. J. Grausem, B. Humbert, and A. Burneau, *Appl. Phys. Lett.* **70**, 1671 (1997).
16. K. Matsuda, S. Nomura, M. Mihara, Y. Aoyagi, S. Nair, and T. Takagahara, *Phys. Rev. Lett.* **91**, 177401 (2003).
17. Y. C. Martin and H. K. Wickramasinghe, *J. Appl. Phys.* **91**, 3363 (2002).
18. B. Hecht, B. Sick, U. P. Wild, V. Deckert, R. Zenobi, O. J. F. Martin, and D. W. Pohl, *J. Chem. Phys.* **112**, 7761 (2000).
19. S. Kawata, M. Ohtsu, and M. Irie, *Nano-Optics* (Springer, Tokyo, 2002), Chap. 4.
20. O. J. F. Martin and C. Girard, *Appl. Phys. Lett.* **70**, 705 (1997).
21. L. Novotny, R. X. Bian, and X. S. Xie, *Phys. Rev. Lett.* **79**, 645 (1997).
22. N. Hayazawa, Y. Inouye, Z. Sekkat, and S. Kawata, *Opt. Commun.* **183**, 333 (2000).
23. N. Hayazawa, Y. Inouye, Z. Sekkat, and S. Kawata, *Chem. Phys. Lett.* **335**, 369 (2001).
24. N. Hayazawa, T. Yano, H. Watanabe, Y. Inouye, and S. Kawata, *Chem. Phys. Lett.* **376**, 174 (2003).
25. R. M. Stöckle, Y. D. Suh, V. Deckert, and R. Zenobi, *Chem. Phys. Lett.* **318**, 131 (2000).
26. A. Hartschuh, E. J. Sánchez, X. S. Xie, and L. Novotny, *Phys. Rev. Lett.* **90**, 095503 (2003).
27. M. S. Anderson and W. T. Pike, *Rev. Sci. Instrum.* **73**, 1198 (2002).
28. W. X. Sun and Z. X. Shen, *Mater. Phys. Mech.* **4**, 17 (2001).
29. L. T. Nieman, G. M. Krampert, and R. E. Martinez, *Rev. Sci. Instrum.* **72**, 1691 (2001).
30. N. Hayazawa, A. Tarun, Y. Inouye, and S. Kawata, *J. Appl. Phys.* **92**, 6983 (2002).
31. K. S. Kunz and R. J. Luebbers, *The Finite-Difference Time-Domain Method for Electromagnetics* (CRC Press, New York, 1993).
32. E. D. Palik, *Hand-Book of Optical Constants of Solids* (Academic Press, London, 1998), p. 286.
33. M. Futamata, Y. Maruyama, and M. Ishikawa, *J. Phys. Chem. B* **107**, 7607 (2003), and references therein.
34. J. B. Pawley, *Handbook of Biological Confocal Microscopy* (Plenum, New York, 1995), 2nd ed.